Lipidomics study in liver metabolic diseases

Singh, M.

Chapter 5

Development of targeted hydrophilic interaction liquid chromatography-tandem mass spectrometry method for acyl-Coenzyme A covering short- to long-chain species in a single analytical run

Based on

Development of targeted hydrophilic interaction liquid chromatography-tandem mass spectrometry method for acyl-Coenzyme A covering short- to long-chain species in a single analytical run

Madhulika Singh, Ligia Akemi Kiyuna, Christoff Odendaal, Barbara M. Bakker, Amy C. Harms, Thomas Hankemeier

Journal of Chromatography A, Volume 1714, 11 January 2024, 464524.
https://doi.org/10.1016/j.chroma.2023.464524

Abstract

Acyl-CoAs play a significant role in numerous physiological and metabolic processes making it important to assess their concentration levels for evaluating metabolic health. Considering the important role of acyl-CoAs, it is crucial to develop an analytical method that can analyze these compounds. Due to the structural variations of acyl-CoAs, multiple analytical methods are often required for comprehensive analysis of these compounds, which increases complexity and the analysis time. In this study, we have developed a method using a zwitterionic HILIC column that enables the coverage of free CoA and short- to long-chain acyl-CoA species in one analytical run. Initially, we developed the method using an LC-QTOF instrument for the identification of acyl-CoA species and optimizing their chromatography. Later, a targeted HILIC-MS/MS method was created in scheduled multiple reaction monitoring mode using a QTRAP-MS detector. The performance of the method was evaluated based on various parameters such as linearity, precision, recovery and matrix effect. This method was applied to identify the difference in acyl-CoA profiles in HepG2 cells cultured in different conditions. Our findings revealed an increase in levels of acetyl-CoA, medium- and long-chain acyl-CoA while a decrease in the profile of free CoA in the starved state, indicating a clear alteration in the fatty acid oxidation process.

Keywords

Acyl-CoA; LC-MS; HILIC; HepG2; Biomarker

1. Introduction

Acyl-CoAs are thioester compounds that have a pivotal role in various metabolic processes such as fatty acid beta-oxidation, biosynthesis of lipids, signaling, and xenobiotics metabolism [1,2]. The most important biological function of acyl-CoAs is in the metabolism of fatty acids via beta-oxidation. The fatty acid beta-oxidation (FAO) process in the liver breaks down fatty acids (FA) to produce adenosine triphosphate (ATP) in low glucose conditions [3,4]. Acyl-CoAs are formed when a FA forms a thioester bond with Coenzyme-A (CoA) [5,6], which subsequently undergo FAO process inside the mitochondria. Fatty acid oxidation disorders (FAOD) occur due to the deficient activity of the enzymes or transporter proteins involved in the pathway, which results in the accumulation of acyl-CoA esters [3]. The acyl-CoA accumulation profile provides information on the type of fatty acid oxidation disorder (FAOD). Intracellular acyl-CoA levels are important reporters of metabolic health and their accumulation in case of FAOD makes them interesting biomarkers [7]. Apart from FAOD, these compounds are also involved in progression of cancer [8–10], diabetes [11–14], precursors for lipid synthesis and ketone bodies. Since acyl-CoA are involved in numerous physiological and pathophysiological pathways, it is important to develop analytical methods for their identification and quantitation.

Developing chromatographic methods for acyl-CoAs is challenging due to their structural complexity. These compounds exhibit significant variations in their physicochemical properties by factors such as carbon chain length, degree of saturation and the presence of functional groups [15–17]. Additionally, acyl-CoAs have low endogenous levels and are highly unstable in aqueous solutions. Due to these reasons they are susceptible to hydrolysis, making sample preparation challenging and resulting in poor recovery and low signal intensity [15,18]. The quantitation of acyl-CoAs has previously been accomplished using a variety of analytical techniques, such as gas chromatography, capillary electrophoresis, and reversed phase liquid chromatography (RPLC) coupled to UV or fluorescence detection [19–22]. However, liquid chromatography coupled to mass spectrometry (LC-MS) is the most widely used technique for acyl-CoA analysis due to its higher sensitivity and selectivity [17–19,23–25]. On the other hand, severe peak tailing, signal deterioration, and poor detection limits are common obstacles associated with this approach [26,27]. Various efforts have been made to cover the full range of acyl-CoAs. In RPLC, slightly acidic mobile phases were used for short- to medium-chain acyl-CoAs [28], while alkaline mobile phase was used for medium- to long-chain acyl-CoAs [26]. Liu et al. used this approach for comprehensive coverage by employing two analytical

runs [23]. The combination of RPLC and hydrophilic interaction liquid chromatography (HILIC) [26] or two-dimensional (2D) LC-MS [17] have also been used to cover short-, medium- and long-chain acyl-CoAs. However, these approaches introduce complexity and increase the analysis time due to the need for multiple chromatographic runs and inclusion of a second dimension of separation. This complexity and added analysis time, in turn, can impact the high-throughput. Another approach for comprehensive coverage is to use ion-pairing reagents such as triethylamine [29] or dimethylbutyl amine [16,25]. However, ion-pairing reagents are reported to decrease mass spectrometry signal intensity [30] and frequent cleaning of detectors is required. Furthermore, a RPLC-MS/MS technique based on phosphate methylation after acyl-CoA derivatization has been reported [15]. Nonetheless, derivatization complicates sample preparation and requires investigation for the evaluation of complete chemical conversion.

HILIC has become increasingly popular and promising for the separation of polar compounds, as HILIC allows class-based separation by hydrophilic interaction. Despite significant variations in chain length polarity, the presence of a similar hydrophilic headgroup in acyl-CoAs facilitates their elution within a relatively shorter time period. In HILIC chromatography, the compounds are separated on a polar stationary phase by gradually increasing mobile phase polarity [31–33]. The compounds with higher polarity have enhanced affinity for the polar stationary phase, thus resulting in prolonged retention, whereas compounds with lower polarity tend to elute earlier.

The aim of the present study is to develop a targeted HILIC-MS/MS method utilizing a zwitterionic HILIC column for the quantitation of free CoA and short- to long-chain acyl-CoA compounds in a single analytical run (covering the full analyte range from high to low polarity) and demonstrate the utility of this method in HepG2 cell application. To achieve this, the initial method development was done on an LC coupled to a high-resolution time-of-flight (QTOF) mass spectrometer (HRMS) for pre-screening of species and evaluating their retention times. The chromatography was optimized by studying the effects of different factors such as buffer concentration and injection solvents. After optimization of various LC-MS settings, a targeted method was created and validation parameters such as linearity, sensitivity, precision, recovery and matrix effect were examined to evaluate method performance in the HepG2 cells. Finally, the HILIC-MS/MS method was applied to compare the free CoA and acyl-CoA profile in HepG2 cells cultured in different conditions.

2. Materials and methods

2.1 Chemicals and reagents

Analytical grade solvents including acetonitrile, chloroform, isopropanol (IPA) and methanol (MeOH) were purchased from Biosolve BV (Valkenswaard, The Netherlands). Purified water was obtained using the Milli-Q Advantage A10 Water Purification System manufactured by Merck Millipore (Billerica, MA, USA). Ammonium acetate with a purity of 99% was supplied by Sigma-Aldrich (St. Louis, MO, USA). Acyl-CoA standards, such as acetyl-CoA (C2:0-CoA) and propionyl-CoA (C3:0-CoA) as sodium salts, octanoyl-CoA (C8:0-CoA), pentadecanoyl-CoA (C15:0-CoA), palmitoyl-CoA (C16:0-CoA), heptadecanoyl-CoA (C17:0-CoA), and 11Z-octadecenoyl-CoA (C18:1(n7)-CoA) as ammonium salts, were purchased from Avanti Polar Lipids (Alabaster, AL, USA). Acetyl-1,2-$^{13}C_2$-CoA (C2:0($^{13}C_2$)-CoA) and n-heptanoyl-CoA (C7:0-CoA) in the form of lithium salts were obtained from Sigma-Aldrich (St. Louis, MO, USA). Additional acyl-CoA standards, including free CoA (CoA), butyryl-CoA (C4:0), hexanoyl-CoA (C6:0), decanoyl-CoA (C10:0), lauroyl-CoA (C12:0), myristoyl-CoA (C14:0), and stearoyl-CoA (C18:0), were provided by collaborators from University Medical Center Groningen (Groningen, The Netherlands).

Dulbecco's Modified Eagle Medium (DMEM) (Product No. P04-01500) and glucose-free DMEM (Product No. P04-01548S1) were purchased from PAN Biotech™. Fetal bovine serum (FBS) and phosphate-buffered saline (PBS) were purchased from Gibco while L-carnitine (Product No. C0283) and palmitate (Product No. P9767) were purchased from Sigma-Aldrich.

2.2 Cell culture

Wildtype HepG2 cells were maintained in DMEM with 5 mM glucose, 3.7 g L^{-1} $NaHCO_3$, 1 mM sodium pyruvate and amino acids, supplemented with 3 mM glutamine, and 10% FBS. The cells were kept at 37 °C and 5% CO_2. To test the individual and combined effects of glucose depletion and fatty acid stimulation on the free CoA level and acyl-CoA profile, the cells were incubated for 24 h in two different conditions. In condition 1 the cells were cultured in DMEM (5 mM glucose, 1 mM pyruvate supplemented with 3 mM glutamine and 10% FBS) with additional supplements 2 mM L-carnitine and 0.5 mM BSA-bound palmitate. Condition 2 was with glucose-free DMEM (no glucose, no glutamine, no pyruvate, 10% FBS) supplemented with 2 mM L-carnitine and 0.5 mM BSA-bound palmitate. After 24 h, the cells were washed twice with ice-cold PBS and harvested for further analysis. Condition 1 cells were

"supplemented cells" with multiple carbon sources, while condition 2 cells were "starved cells" with fewer carbon sources.

2.3 Sample preparation

Acyl-CoAs from HepG2 cells were extracted by a two-step protocol using chloroform/methanol/water based on the Bligh and Dyer approach [34]. 10 µL of acyl-CoA internal standard (IS) containing mixture of C2:0($^{13}C_2$)-CoA, C7:0-CoA, C15:0-CoA and C17:0-CoA with concentration of 3 µM were spiked in the HepG2 cell extracts containing 1×10^6 cells in 100 µL of methanol. To this extract, 220 µL of cold methanol and 100 µL of cold water was added and sonicated for 3 min. After sonication, 320 µL of chloroform and 188 µL of cold water was added. Samples were vortexed for 2 min, left to partition on ice for 10 min, and centrifuged at 15800 rcf for 15 min at 4 °C. 450 µL of the upper aqueous layer was transferred to a new Eppendorf tube. Samples were evaporated to dryness with a Labconco CentriVap vacuum concentrator (Kansas City, MO, USA). The dried samples were reconstituted in 100 µL of methanol/water/isopropanol (1:1:1), vortexed and centrifuged for 10 min. The supernatant was transferred to HPLC vial for LC-MS analysis.

2.4 HILIC-HRMS (HILIC-TOF-MS) analysis

The Waters Synapt G2-S quadrupole time-of-flight mass spectrometer with an electrospray ionization (ESI) source (Milford, MA, USA) was coupled to an Acquity UPLC system (Waters). The chromatographic separation was performed on SeQuant® ZIC®-cHILIC (100 mm x 2.1 mm, 100 Å pore size, 3 µm) column. The column oven and autosampler temperatures were set at 40 ^{o}C and 10 ^{o}C respectively. Mobile phase A (MP-A) consisted of acetonitrile:water (9:1) containing 5 mM ammonium acetate and acetonitrile:water (1:9) with 5 mM ammonium acetate was used for mobile phase B (MP-B). The flow rate was 0.25 mL/min and injection volume was 5 µL. The gradient program is shown in **Table S1**. The autosampler injection needle was washed with a weak needle wash consisting of acetonitrile:water (9:1, v/v) and strong needle wash consisting of acetonitrile:water (1:9, v/v).

For the MS analysis, a TOF-MS scan was performed. The mass spectrometer was set to scan a mass range from 300 to 1200 Da in both positive and negative ESI ionization modes. To ensure accurate mass measurement, 0.1 mg/L leucine-enkephalin in water:MeOH:formic acid (50:50:0.1, v/v/v) was used as a lock-mass calibrant with the infusion flow rate of 10 µL/min. The mass spectrometer was operated with the following parameters: the capillary voltage was set at 2.50 kV in both positive and negative mode of ionization; the sampling cone voltage was

set to 30 V and the source offset voltage was 100 V. The source temperature was maintained at 125 °C, while the desolvation temperature was set at 500 °C. Gas flows were controlled as follows: the cone gas flow rate was set to 50 L/h; the desolvation gas flow rate was 500 L/h, and the nebulizer gas flow rate was adjusted to 6 Bar.

2.5 HILIC-QTRAP (HILIC-MS/MS) analysis in scheduled MRM mode

The targeted HILIC-MS/MS analysis was performed on a Waters Acquity UPLC I-class system from Waters (Milford, MA, USA) coupled to an AB Sciex QTRAP 6500 mass spectrometer (Concord, ON, Canada). The needle wash was acetonitrile:water (1:1, v/v). The column, mobile phase, autosampler temperature and column oven temperature were the same as described in section *2.4.* with a slight modification in the gradient program as shown in **Table 1**.

Table 1. Gradient for HILIC-MS/MS analysis.

Time (min)	Flow rate (mL min^{-1})	MP-A (%)	MP-B (%)
Initial	0.25	95	5
2.3	0.25	95	5
8.5	0.25	25	75
13.00	0.25	15	85
15.5	0.25	15	85
15.6	0.25	95	5
20	0.25	95	5

The MS/MS experiments were conducted on a Turbo V source. The analysis was conducted in positive ion mode and analytes were monitored in scheduled multiple reaction monitoring (sMRM) mode. The mass spectrometer was operated at the following settings: the curtain gas (N_2) pressure was set to 25 psi, and the collision gas (N_2) was maintained at a medium level. The spray voltage was set at 4000 V in positive ion mode. The source temperature was maintained at 325 °C. The GS1 and GS2 pressures both were set at 60 psi. The target scan time was of 0.35 sec. The delustering potential (DP) and collision energy (CE) were optimized to achieve maximum response.

2.6 Method validation

Method validation of the HILIC-MS/MS method was performed using non-endogenous acyl-CoA standards- C2:0($^{13}C_2$)-CoA, C7:0-CoA, C15:0-CoA and C17:0-CoA. These standards were either isotopically labeled or had odd chains to be free from interference of endogenous species.

2.6.1 Calibration curves

The calibration curves were freshly prepared on three different days to assess the linearity of the method. For this purpose, an 8-point calibration line was created by serially diluting the standards. The concentrations of these calibration points are presented in **Table S2**. Three types of calibration lines were prepared: 1) Neat solvents; 2) Spiking standards in HepG2 cells before performing the extraction as described in the sample preparation section; 3) Spiking standards in HepG2 cells after extraction. To determine the linear range, an unweighted linear regression model was employed. The calculation of various validation parameters was performed using cal-3 (low), cal-5 (medium), and cal-7(high) concentration levels.

2.6.2 Limit of detection (LOD) and limit of quantitation (LOQ)

LOD and LOQ were calculated by using equation 1 and equation 2 respectively.

$$LOD = \frac{3 \times SD_{area C_{S/N>3}} + area_{blank}}{\frac{area_{C_{S/N>3}}}{[C_{S/N>3}]}} \quad (1)$$

$$LOQ = \frac{10 \times SD_{area C_{S/N>3}} + area_{blank}}{\frac{area_{C_{S/N>3}}}{[C_{S/N>3}]}} \quad (2)$$

where $SD_{area C_{S/N>3}}$ represents the standard deviation of area of the lowest concentration with signal-to-noise ratio greater than 3($C_{S/N>3}$), $area_{blank}$ are the peak area of the blank and $\frac{area_{C_{S/N>3}}}{[C_{S/N>3}]}$ represents the ratio between peak area and concentration at $C_{S/N>3}$ [35].

2.6.3 Precision

Precision was assessed by calculating the relative standard deviation (RSD %). Low, medium and high concentration levels were used for this analysis. Intraday precision was determined by conducting three consecutive measurements on the same day. Interday precision, on the other hand, was evaluated by measuring the samples on three different days. The precision was calculated by equation 3 [36].

$$RSD\ (\%) = \frac{Standard\ deviation}{Mean} \times 100 \quad (3)$$

2.6.4 Extraction Recovery

The response of standards at low, medium and high levels (measured in triplicate) was calculated in the samples spiked before and after extraction in HepG2 cells and equation 4 was used to calculate the recovery.

$$Recovery(\%) = \frac{Response\ of\ standards\ in\ HepG2\ cells\ before\ extraction}{Response\ of\ standards\ in\ HepG2\ cells\ after\ extraction} \times 100 \quad (4)$$

2.6.5 Matrix effect

Matrix effect is a prevalent issue encountered in mass spectrometry measurements. It refers to a phenomenon where the response of an analyte is suppressed or amplified due to the presence of a matrix or other interfering components that affect the ionization process of compounds. This was calculated by equation 5 at low, medium and high level (measured in triplicate).

$$Matrix\ effect(\%) = \frac{Response\ of\ standards\ in\ HepG2\ cells\ after\ extraction}{Response\ of\ standards\ in\ neat\ solvents} \times 100 \quad (5)$$

2.6.6 Carryover

Carryover refers to the presence of analytes in the blank samples after injection of the highest calibration standards [37]. This was evaluated by comparing the peak area of standards in the blank solvents to the peak area of standards spiked in high concentration in HepG2 cells, analyzed before the blank solvents.

2.6.7 Repeatability

The repeatability of our method was assessed by calculating RSD (%) of endogenous acyl-CoA species in the quality control (QC) samples inserted at regular intervals in the batch of study samples.

2.7 Quantitation

The odd-chain or isotopic labeled non-endogenous standards were used as internal standards for the quantitation of endogenous acyl-CoA species. C2:0($^{13}C_2$)-CoA was used for the quantitation of short-chain species, C7:0-CoA was used for the quantitation of medium-chain species while C15:0-CoA and C17:0-CoA were used for the quantitation of long-chain species. These standards were used for the quantitation of both saturated and unsaturated species. In this study, we find that the abundance of unsaturated species in the biological samples was very low and hence their contribution to isotopic interference was less than 1%. Therefore, we do not require any isotopic correction in this study.

2.8 Data processing

Data acquisition was performed using MassLynx (version 4.1) for the Synapt G2-S (HILIC-TOF-MS) and Analyst (version 1.6.2) for the QTRAP (HILIC-MS/MS). Peak integration was performed using TargetLynx (version 4.1) and Sciex OS (version 2.1.6) for HILIC-TOF-MS and HILIC-MS/MS respectively. The peak asymmetry factor was used to determine the effect of different conditions during method development and was calculated by equation 6 [38].

$$A_s = b/a \qquad (6)$$

where A_s = peak asymmetry factor, b = half width of peak (distance from peak midpoint to the trailing edge at 10% of the full peak height), a = front half width (distance from peak midpoint to leading edge at 10% of the peak height). A_s is lower than 1 for a fronting peak and higher than 1 for a tailing peak.

GraphPad Prism (version 9) was used to calculate statistical significance between the groups using t-test and plot graphs.

3. Results and Discussion

Representative standards C2:0-CoA (short-chain), C8:0-CoA (medium-chain), C16:0-CoA and C18:1-CoA (long-chain) from each chain length were used for method optimization.

3.1 Mass spectrometry parameters optimization

The TOF-MS scan on the Synapt G2-S was performed in both positive ESI mode (ESI^+) and negative ESI (ESI^-) mode by injecting a mixture of four representative acyl-CoA standards. Firstly, the observed mass of the representative standards was confirmed with their accurate masses in protonated $[M+H]^+$, deprotonated $[M-H]^-$ and doubly charged negative ions $[M-2H]^{2-}$ form. The corresponding m/z values of these acyl-CoA standards are presented in **Table S3** and the sensitivity of acyl-CoA standards in different ionization modes is shown in **Figure S1.** Doubly charged ions in the negative mode $[M-2H]^{2-}$ have slightly higher sensitivity for these standards compared to their protonated form $[M+H]^+$ while intensities were very low in singly negative charged ion $[M-H]^-$. Despite the slightly higher sensitivity observed in the doubly charged ions in negative mode, we decided to measure protonated species utilizing positive ionization mode for our analysis. This choice was based on the previously reported studies [16–18] and the fragmentation patterns observed in positive ionization mode provide a more straightforward approach for analyzing acyl-CoAs. Additionally, when dealing with doubly charged negative ions, there may be greater susceptibility to background interference, which

can disrupt the linearity of the analysis. **Table S4** presents the observed m/z of all the targets with their retention times in the HILIC-TOF-MS method.

3.2 Chromatographic separation for acyl-CoAs

We started the chromatographic separation with a 20 min long gradient elution as reported in **Table S1.** In order to achieve the quantitation of all acyl-CoA species in a single analytical run, we employed a ZIC-cHILIC column which contains a phosphorylcholine group **(Figure S2)** that consists of a negatively charged inner moiety and a positively charged outer moiety [39]. We chose to use this ZIC-cHILIC column for the chromatography optimization of acyl-CoA as it was reported to effectively separate various compounds containing phosphate groups like ATP, ADP, NAD, sugar phosphates, etc. [40–42]. The presence of a zwitterionic stationary phase requires lower concentrations of buffer compared to other types of stationary phases, as the zwitterionic stationary phase contains both positive and negative charges. This causes weak electrostatic interactions with the analytes and hence only a low concentration of buffer is needed [39]. The peak tailing observed in the acyl-CoA species can be attributed to the presence of the phosphate group on CoA moiety [43]. This phenomenon might occur due to the interactions of phosphate groups and metal surfaces in path of LC flow [44]. Additionally, these phosphate groups have a tendency to adhere to the stainless steel parts of the LC-MS instrumentation, further contributing to the challenges in analysis [43]. The buffer salts such as ammonium acetate and ammonium formate are known to maintain the ionization of analytes and decrease the interaction between stationary phase and analytes [31,45–47]. We have used ammonium acetate buffer as this is one of the most commonly used buffers for metabolomics studies employing HILIC chromatography [46–48]. In this study, we investigated the impact of different concentrations of ammonium acetate on the peak shape, separation and retention of acyl-CoAs. Mobile phases were prepared with concentrations of 2.5 mM, 5 mM, and 10 mM ammonium acetate and the buffer concentration was kept same in both mobile phases to maintain consistent ionic strength throughout the gradient elution. **Figure 1** displays the peaks of the acyl-CoA standards for each buffer concentration and peak asymmetry factors were calculated and summarized in **Table 2**. Notably, as the concentration of ammonium acetate increased, the peak tailing of the acyl-CoAs decreased. After evaluating different concentrations of ammonium acetate, a final concentration of 5 mM was chosen, as it resulted in satisfactory peak shapes. Additionally, maintaining a lower salt concentration helps in preventing excessive salt precipitation within the instrument, ensuring its proper functionality and long-term stability. Furthermore, we assessed the influence of pH variation and flow rate

on peak tailing but did not observe any significant effects (data not shown). As a result, a flow rate of 0.25 mL/min was chosen for chromatographic separation with the presence of 5 mM ammonium acetate in the mobile phases.

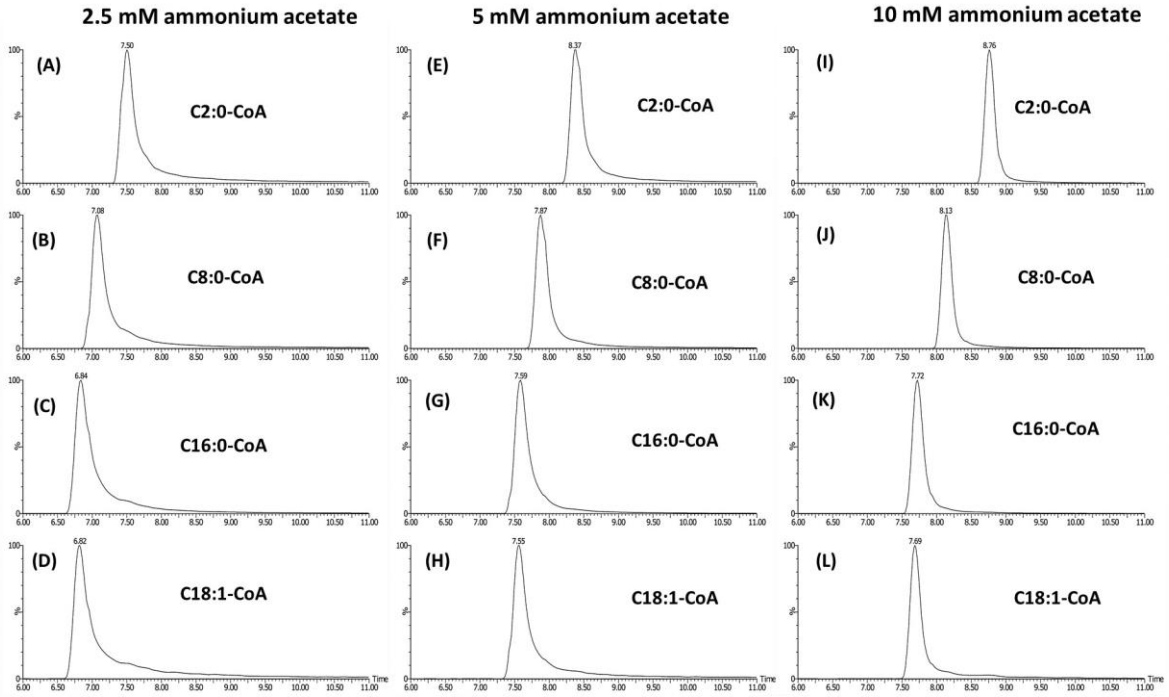

Figure 1. Extracted ion chromatograms of representative acyl-CoA standards (C2:0-CoA, C8:0-CoA, C16:0-CoA and C18:1-CoA) separated in mobile phases containing 2.5 mM ammonium acetate (A-D), 5 mM ammonium acetate (E-H) and 10 mM ammonium acetate (I-L). X-axis represents time (min) and Y-axis represents intensity.

Table 2. Peak asymmetry factor of acyl-CoA standards with 2.5 mM ammonium acetate, 5 mM ammonium acetate and 10 mM ammonium acetate.

Concentration of ammonium acetate (mM)	C2:0-CoA	C8:0-CoA	C16:0-CoA	C18:1-CoA
2.5	7.00	5.71	6.38	6.78
5	4.29	3.29	4.38	2.57
10	3.40	2.14	2.57	1.78

Further, we tested the effect of cell matrix on peak tailing by spiking four representative acyl-CoA standards in HepG2 cells after extraction. The ammonium acetate concentration of the mobile phase was kept at 5 mM, and peak asymmetry factor was compared between acyl-CoA standards spiked in the cell samples and the neat standards. It was observed that peak tailing and subsequently asymmetry factor has been reduced due to the presence of cell matrix **(Figure 2, Table 3)**. One possible explanation behind the reduction of peak tailing in the presence of

cell matrix is that the components within the cell samples can act as masking agents, thus disrupting the secondary interactions between analytes and LC system. As a result, the interaction between the acyl-CoA molecules and the column is reduced, leading to a decrease in peak tailing during chromatographic analysis. However, additional investigations are required to confirm this hypothesis. This can also be valuable as understanding the role of the cell matrix in reducing peak tailing can provide valuable insights for optimizing analytical methods and can be helpful in developing strategies to minimize peak tailing and improve the overall performance of chromatographic analyses.

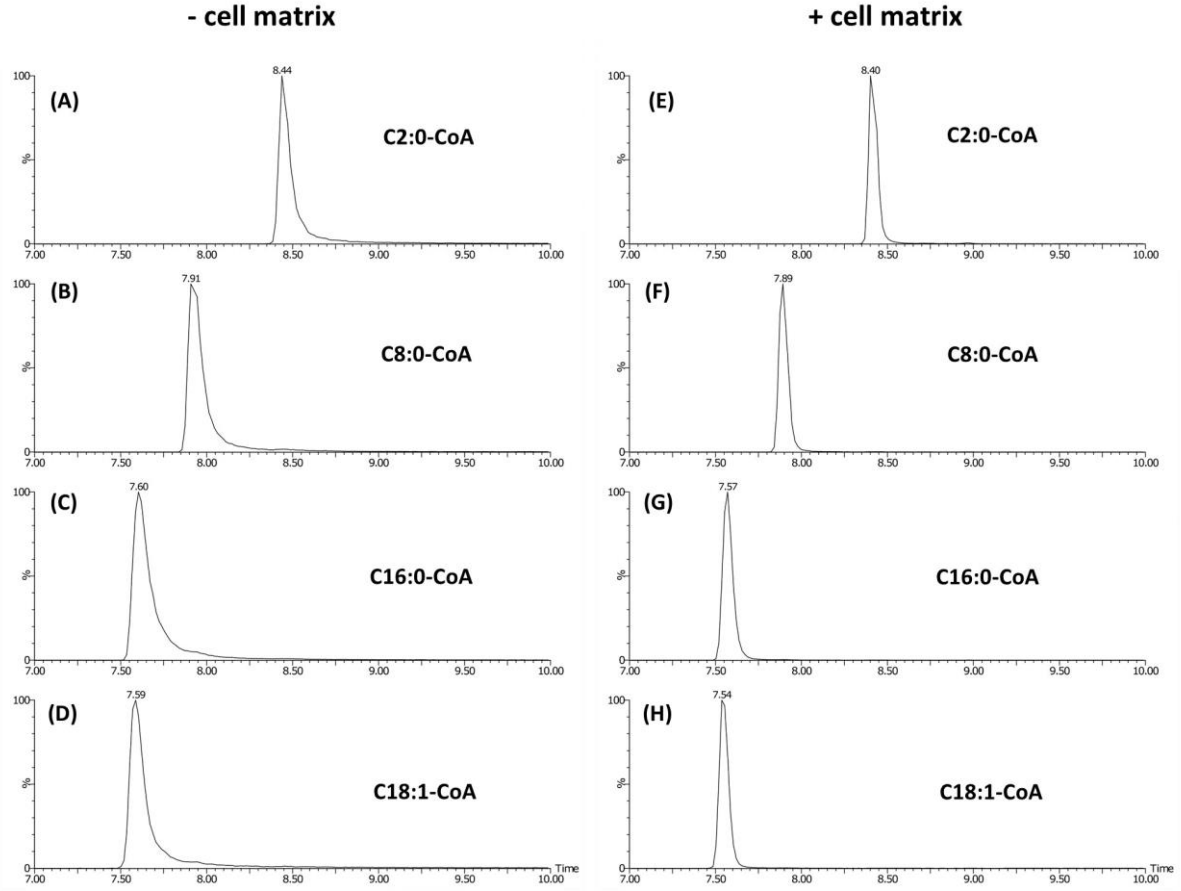

Figure 2. Extracted ion chromatograms of representative acyl-CoA standards (C2:0-CoA, C8:0-CoA, C16:0-CoA and C18:1-CoA) in 5 mM ammonium acetate, without (A-D) and with (E-H) cell matrix. X-axis represents time (min) and Y-axis represents intensity.

Table 3. Peak asymmetry factor of acyl-CoA standards with and without cell matrix.

Cell matrix	C2:0-CoA	C8:0-CoA	C16:0-CoA	C18:1-CoA
Absent (-)	2.32	2.00	3.50	2.28
Present (+)	2.00	1.40	1.33	1.60

3.3 Optimization of injection solvent for sample reconstitution

Acyl-CoAs are highly unstable in alkaline and strongly acidic solutions [18]. It is important to check the stability of acyl-CoAs in the injection solvents to assess degradation rate and determining the time window for stable sample analysis. As mentioned previously in literature, methanol was considered to have good stability for acyl-CoA for 24 h [18]. For this experiment, the four representative acyl-CoA standards (C2:0-CoA, C8:0-CoA, C16:0-CoA and C18:1-CoA) were reconstituted in 5 different solutions, MeOH:Water (1:5,v/v), MeOH:Water:IPA (1:1:1,v/v/v), MeOH:50 mM ammonium acetate (1:1,v/v), MeOH:Water (1:1,v/v) and methanol (100%). The presence of water in the injection solvents is necessary for the solubility of acyl-CoA especially for the short-chain species. The four acyl-CoA standards were dissolved in solvents, placed in the autosampler, and analyzed with the HILIC-TOF-MS method at three different time points: 0 h, 6 h and 24 h **(Figure 3).**

The stability of acyl-CoAs in the various solvents was assessed by measuring the change in response at 6 and 24 h, expressed as a percentage relative to the response observed at 0 h. Both MeOH:Water (1:5, v/v) and MeOH:Water:IPA (1:1:1, v/v/v) showed acceptable stability over time for the acyl-CoAs. The response with the injection solvent MeOH:50 mM ammonium acetate (1:1,v/v) decreased at 6 and 24 h, except for C2:0-CoA, which had a higher response at these time points. MeOH:Water (1:1,v/v) and methanol (100%) showed increase in response at 24 h as compared to 6 h especially for C2:0-CoA and C8:0-CoA. Methanol (100%) also shows a high variation in response for C2:0-CoA. The exact reason behind this observation is not clearly understood, however, solubility could be one of the contributing factors. For our method, we chose methanol:water:isopropanol (1:1:1, v/v/v) as the injection solvent as it has acceptable stability and the inclusion of slightly less polar solvent (isopropanol) in the injection solvent can increase the solubility of long-chain acyl-CoAs.

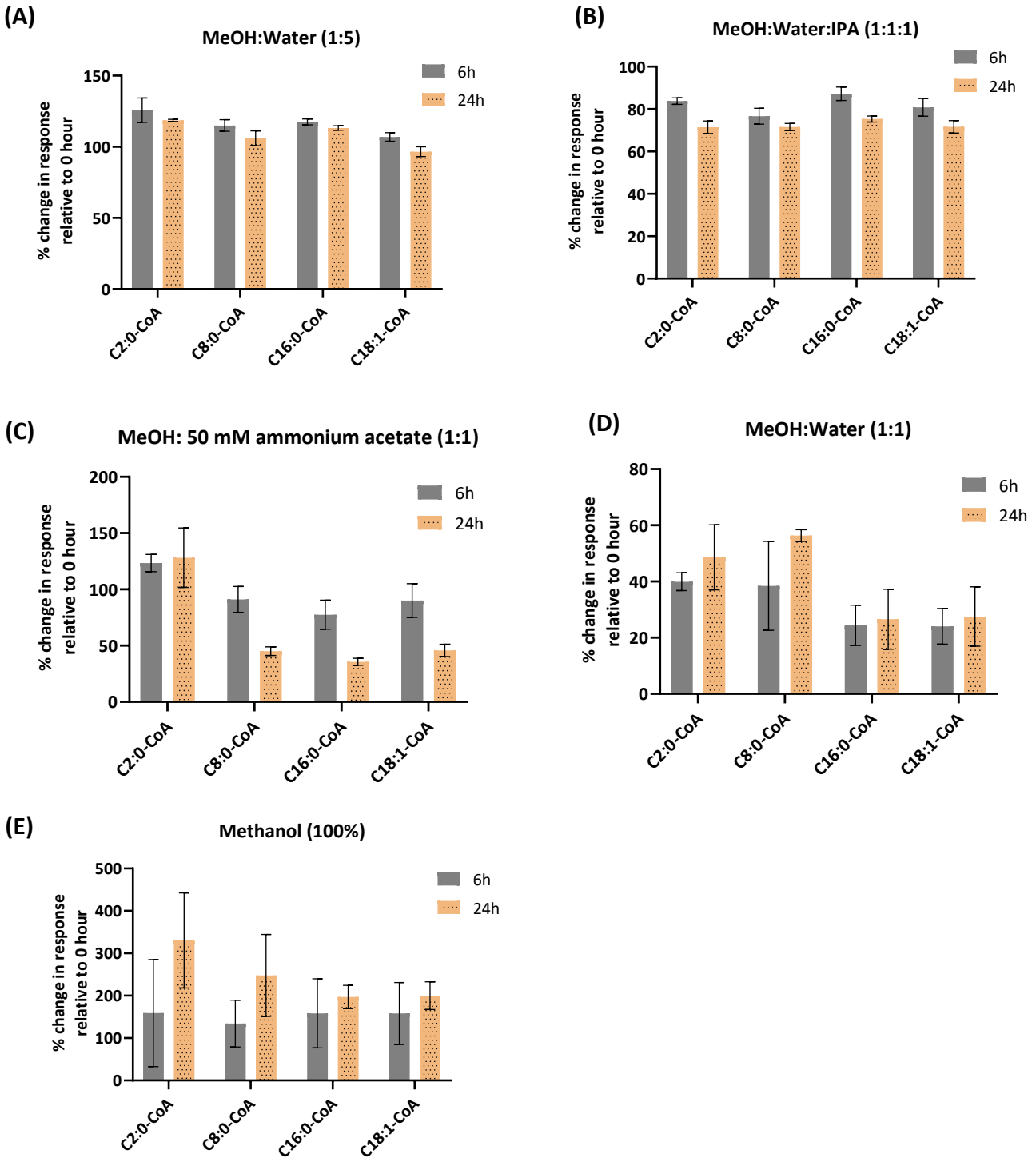

Figure 3. Stability of representative acyl-CoA standards (C2:0 CoA, C8:0 CoA, C16:0 CoA and C18:1 CoA) in different injection solvents. (A) MeOH:Water (1:5, v/v); (B) MeOH:Water:IPA (1:1:1, v/v/v); (C) MeOH:50 mM ammonium acetate (1:1, v/v); (D) MeOH:Water (1:1, v/v); (E) Methanol (100%).

3.4 HILIC-MS/MS QTRAP analysis

Following the optimization of chromatographic and mass spectrometry conditions, a targeted method was created using the sMRM mode on the QTRAP instrument in positive ion mode. We made slight modifications and finalized the gradient program as presented in **Table 1**. The formation of water-rich layer on the surface of stationary phase is quite important for interaction with the analytes to ensure consistent retention of compound. Hence, we specifically extended the equilibration time as it is a critical step in HILIC for a stable chromatography. **Figure 4(A)** shows the representative chromatogram of acyl-CoA standards.

The fragmentation pattern was examined for the selection of product ion (Q3). Acyl-CoA species exhibit two important fragments [15,17–19]. The first is the neutral loss of 507 Da $[M+H-507]^+$, which occurs as a result of the loss of the 3'-phosphate-adenosine-5'-diphosphate moiety from the acyl-CoA precursor molecular ion. Additionally, m/z 428 is another distinctive fragment present in all acyl-CoA species which is the representative CoA moiety. These findings were confirmed in **Figure 4(B),** which presents the fragmentation pattern of C7:0-CoA. **Figure 4(C)** illustrates the structural sites for fragmentation of acyl-CoA. The neutral loss of 507 was chosen as the product ion (Q3) for the sMRM mode as it was the most intense and common fragment among acyl-CoAs, as observed in our study and supported by other publications [15,19].

In the HILIC-TOF-MS method, the focus was primarily on detecting saturated species, however with the use of highly sensitive QTRAP instrument we were able to detect a few additional monounsaturated species. The identification of these monounsaturated species was confirmed by evaluating the pattern of their retention times (**Figure 5**). The intensity of these species was much lower compared to their saturated form, nevertheless their detection can provide additional information and contribute to understanding the biological context of the study samples. The targets along with their sMRM parameters have been mentioned in **Table 4.**

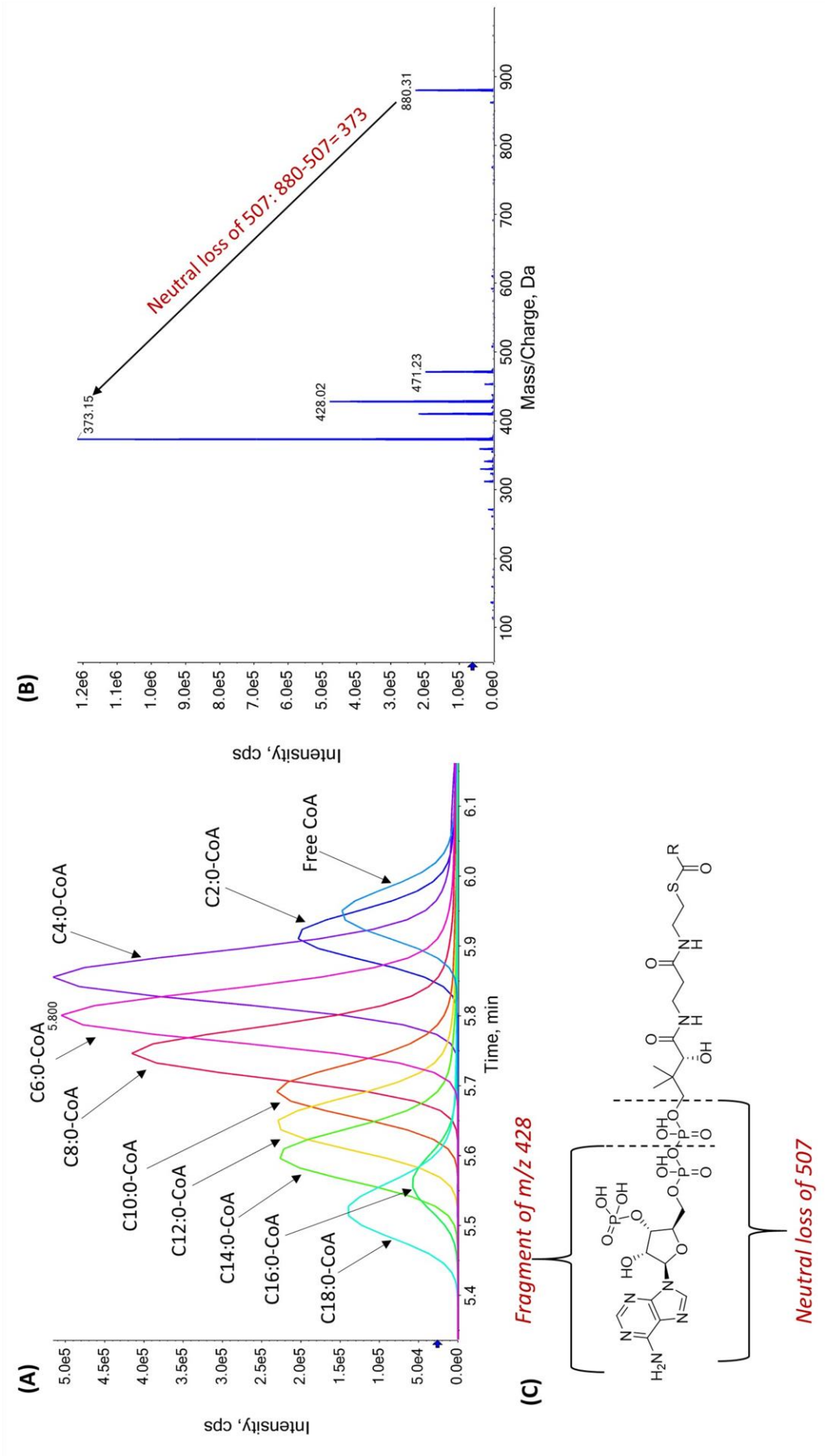

Figure 4. (A) Representative chromatogram of acyl-CoA standards; (B) Mass spectrum showing fragmentation of C7:0-CoA; (C) Structural sites of acyl-CoA fragmentation.

Table 4. sMRM parameters for acyl-CoA targets in HILIC-MS/MS method.

Targets	Q1	Q3	RT	DP	CE
CoA (Free CoA)	768.1	261.1	5.99	100	40
C2:0-CoA (Acetyl-CoA)	810.1	303.1	5.95	100	40
C3:0-CoA (Propionyl-CoA)	824.2	317.2	5.90	100	40
C4:1-CoA	836.2	329.2	ND	100	40
C4:0-CoA	838.2	331.2	5.88	100	40
C6:1-CoA	864.2	357.2	ND	100	40
C6:0-CoA (Hexanoyl-CoA)	866.2	359.2	5.82	100	40
C8:1-CoA	892.2	385.2	5.79	100	40
C8:0-CoA(Octanoyl-CoA)	894.2	387.2	5.76	100	40
C10:1-CoA	920.2	413.2	5.72	100	40
C10:0-CoA (Decanoyl-CoA)	922.3	415.3	5.71	100	40
C12:1-CoA	948.3	441.3	5.68	100	45
C12:0-CoA (Lauroyl-CoA)	950.3	443.3	5.65	100	45
C14:1-CoA	976.3	469.3	5.63	100	45
C14:0-CoA (Myristoyl-CoA)	978.3	471.3	5.61	100	45
C16:1-CoA	1004.3	497.3	5.59	100	45
C16:0-CoA (Palmitoyl-CoA)	1006.4	499.4	5.56	100	45
C18:1-CoA	1032.4	525.4	5.55	100	45
C18:0-CoA (Steraoyl-CoA)	1034.4	527.4	5.54	100	45
C2:0-CoA($^{13}C_2$) (Acetyl-1,2-$^{13}C_2$-CoA)*	812.1	305.1	5.95	100	40
C7:0-CoA (Heptanoyl-CoA)*	880.2	373.2	5.78	100	40
C15:0-CoA (Pentadecanoyl-CoA)*	992.3	485.3	5.58	100	45
C17:0-CoA (Heptadecanoyl-CoA)*	1020.4	513.4	5.55	100	45

*, Internal standard; ND, not detected

3.5 Retention time pattern

The identification and confirmation of acyl-CoA species were further supported by analyzing their retention time pattern. In HILIC chromatography, the gradient initiates with an organic mobile phase and subsequently transitions to a more aqueous phase. As a result, acyl-CoA species with longer carbon chains elute first, followed by medium- and short-chain species, as depicted in **Figure 5.** Similarly, species with a higher number of double bonds but the same number of carbon atoms elute later compared to species with a lower number of double bonds. For example, C16:0-CoA elutes at 5.56, while C16:1-CoA elutes at 5.59. This distinct retention time pattern is highly valuable for the identification and confirmation of a wide range of acyl-CoA species.

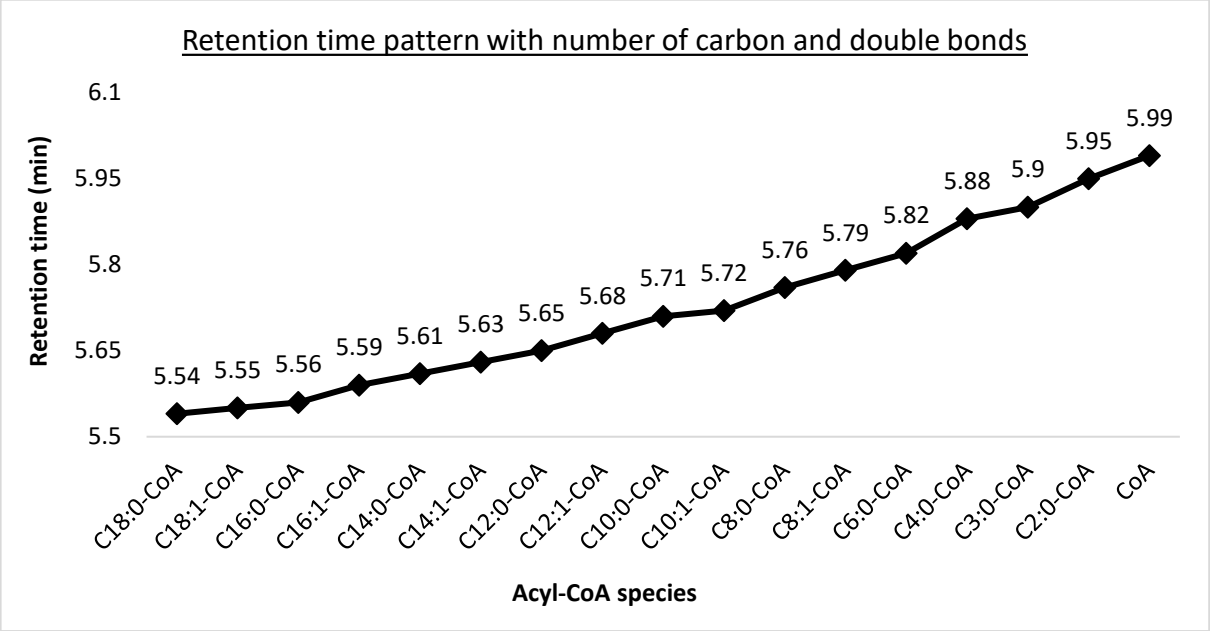

Figure 5. Retention time pattern of acyl-CoA species.

3.6 Method validation of targeted HILIC-MS/MS method

The targeted HILIC-MS/MS method was validated for quantitation of acyl-CoA compounds in HepG2 cells. Representative non-endogenous standards from short-(C2:0($^{13}C_2$)-CoA), medium-(C7:0-CoA) and long-chain (C15:0-CoA and C17:0-CoA) species were chosen for the validation. The calibration curves of non-endogenous standards spiked in pure solvent and in HepG2 cells (before and after extraction) are shown in **Figure 6.** The values of linearity, LOD, LOQ, precision, recovery, matrix effect and carryover are reported in **Table 5**. The linear regression coefficients (R^2) were above 0.99 for all spiked standards. The LODs and LOQs were in the range of (1.3-12.4) pmol mL^{-1} and (3.1-26.6) pmol mL^{-1} respectively which makes our method sensitive enough to detect the acyl-CoAs in ~1×10^6 HepG2 cells. In comparison to

previous studies, reporting LODs in the range of (0.5-2.4) pmol mL^{-1} [26], (3-133) pmol mL^{-1} [7] and (1.2-4.6) pmol mL^{-1} [15], our reported LODs were comparable and, in some cases, even lower. It is worth noting that in our method development, we tried to achieve sensitivity without compromising on reliability and throughput. The intraday and interday precisions were determined at low, medium and high concentration levels. Almost all the classes have RSD (%) below 20% except for C15:0 CoA with slightly higher value of 22.9% at low level. The recovery was in the range of (53-123)% for all standards. It was observed that recovery of long-chain acyl-CoA species is slightly lower. The reason for this may be that long-chain acyl-CoA species have lower polarity compared to short- and medium-chain species, which could result in their migration to the non-polar lower layer. The matrix effect was in the range of (85-133)%. The carryover was analyzed in the blank samples placed right after the highest calibration point in HepG2 cells before extraction and was below 1% for all standards. We are using non-endogenous compounds as internal standards based on the chain length of endogenous targets. These standards elute in close proximity to the endogenous compounds present in the sample. Hence, the issues related to poor recovery, ion suppression and matrix effects can be compensated as internal standards and endogenous compounds will parallelly go through the same processing.

The repeatability evaluates the consistency and reliability of the results, ensuring that there is minimal deviation or variability in the analysis. The repeatability of our HILIC-MS/MS method was determined by measuring the RSD (%) of endogenous acyl-CoA species in QC samples. It was found that out of 19 targets, 7 species show RSD below 5%. The RSD of (5-10)% and (10-15)% was shown by 7 and 1 species respectively while 2 species show RSD in between (15-25)%. Two species were not detected in these samples. In total, 17 acyl-CoA species show RSD below 25% **(Figure S3).** We further tested the stability of non-endogenous acyl-CoA standards in HepG2 cells over 3 days. The extracted samples of HepG2 cells containing these standards were analyzed on day 1. The samples were then stored at -80 °C and analyzed again on day 3. We compared the peak area of these standards on both days **(Table S5)** and found that the deviation over 3-day period, ranges from (5-10)%, indicating good stability during this time. However, for a more comprehensive assessment, further experiments are required by storing samples for longer periods under different conditions.

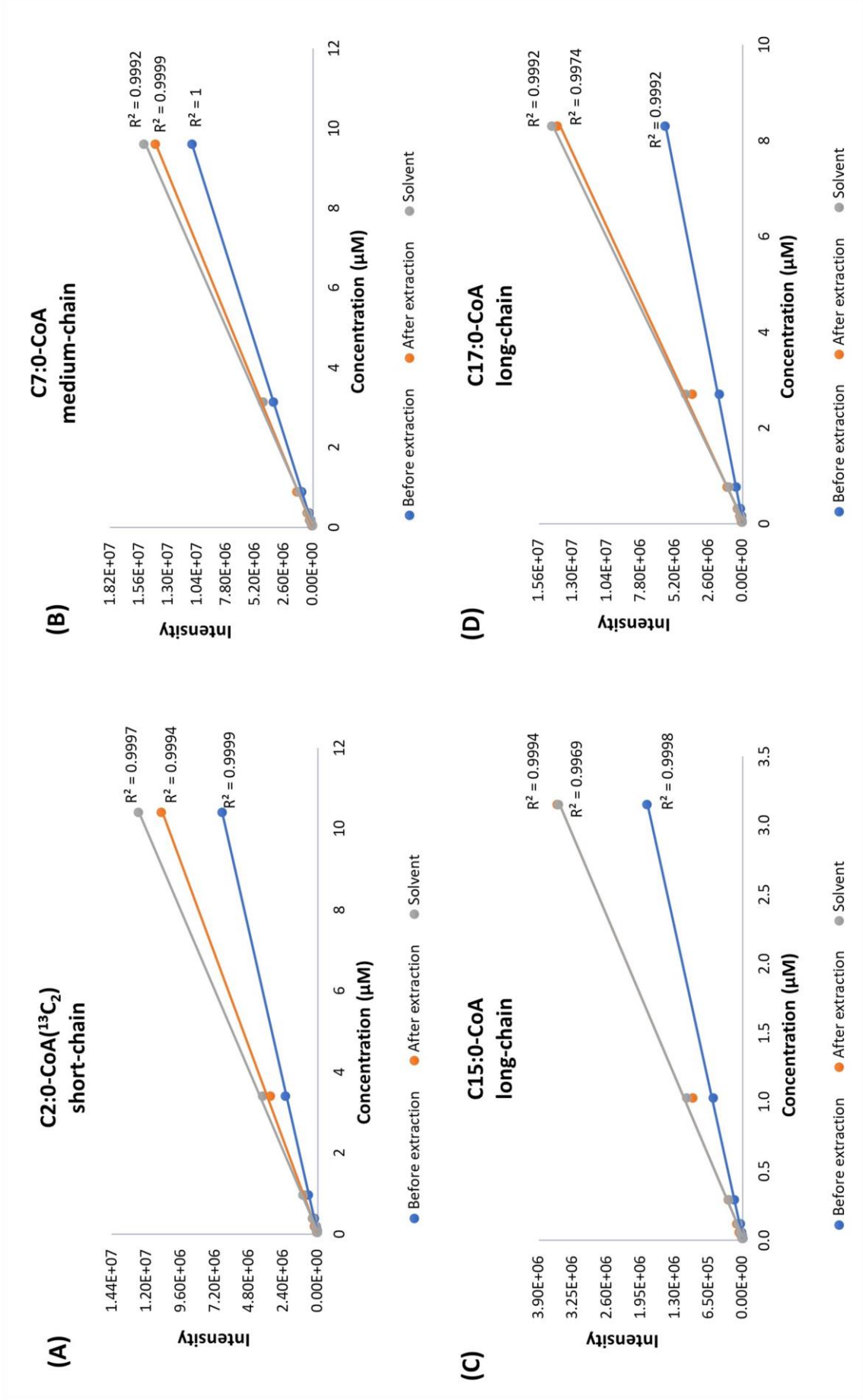

Figure 6. Calibration curves of non-endogenous acyl-CoA standards spiked in pure solvent, spiked in HepG2 cells before and after extraction. (A) C2:0-CoA($^{13}C_2$): short-chain; (B) C7:0-CoA: medium-chain; (C) C15:0-CoA: long-chain; (D) C17:0-CoA: long-chain.

Table 5. Summary of the validation parameters.

Non-endogenous acyl-CoA standards	Linearity	LOD (µM)	LOQ (µM)	Intraday precision [%]			Interday precision [%]			Recovery [%]			Matrix effect [%]			Carryover [%]
				Low	Medium	High	Low	Medium	High	Low	Medium	High	Low	Medium	High	
C2:0-CoA($^{13}C_2$)	0.9999	0.0013	0.0031	2.2	2.2	1.0	4.7	3.3	2.5	100.0	88.7	92.2	114.7	101.4	85.7	0.4
C7:0-CoA	1	0.0076	0.0136	4.1	3.4	5.2	12.7	17.4	20.3	123.4	100.1	105.4	124.8	113.0	101.1	0.3
C15:0-CoA	0.9998	0.0110	0.0266	9.5	6.5	4.4	22.9	14.2	11.4	73.1	62.0	80.3	129.9	122.2	89.5	0.3
C17:0-CoA	0.9992	0.0124	0.0230	7.0	5.7	3.0	18.4	6.2	14.1	80.9	53.5	62.5	133.1	113.6	89.0	0.2

3.7 Acyl-CoA profile in HepG2 cells cultured in supplemented and starved state

We applied our HILIC-MS/MS method to analyze acyl-CoA profile of wildtype HepG2 cells cultured under two different conditions. In Condition 1 (supplemented cells), the cells were cultured in a medium containing glucose, pyruvate, glutamine with supplementation of carnitine and palmitate. On the other hand, Condition 2 (starved cells) involved culturing the cells in a glucose-free medium with no pyruvate and glutamine, but with the addition of carnitine and palmitate, aiming to simulate a state of starvation. **Figure 7(A)** shows the profile of free CoA and short- to long-chain acyl-CoAs in HepG2 cells cultured under both supplemented (condition 1) and starved conditions (condition 2). **Figure 7(B)** displays the fold change in acyl-CoA levels between the supplemented and starved states. We observed a decrease in the free CoA level ($p<0.05$) during the starvation state of HepG2 cells while there has been an increase in the acetyl-CoA ($p<0.0001$) in starved cells as compared to supplemented ones. The medium chain acyl-CoA also showed an increase in their profile in starved conditions for C6:0-CoA ($p<0.0021$), C8:0-CoA ($p<0.05$) and C10:0-CoA ($p<0.0002$). Furthermore, we observed an increase in the profile of long-chain acyl-CoA such as C12:0-CoA, C14:0-CoA and C16:0-CoA with $p<0.0001$.

The change in the profile of acyl-CoAs in our study shows an activation of fatty acid oxidation. During starvation conditions, cells shift in the survival mode due to decrease in glucose level, activating the FAO process. In FAO, free fatty acids are activated to long-chain acyl-CoA and enter inside the mitochondria for fatty acid oxidation process, thus leading to an increase in the level of long-chain acyl-CoA. A study has reported an increase in the expression of acyl-CoA synthetase (ACS) and carnitine palmitoyltransferase-1 (CPT-1) while decrease in the level of acetyl-CoA carboxylase (ACC) during fasting conditions [49]. ACS increases the formation of fatty acyl-CoA from fatty acid and CPT-1 is responsible for converting acyl-CoAs into acylcarnitines. The increase in the level of both of these enzymes suggests an increase in the transportation of long-chain acyl-CoA inside mitochondria. Our data also reflects the same with increase in the profile of long-chain acyl-CoAs in the starved state. On the contrary, ACC controls the rate-limiting step of FAO by facilitating the formation of malonyl-CoA, an inhibitor of CPT-1. The decrease in its level further supports the formation of long-chain acyl-CoA. Acetyl-CoA (C2:0-CoA) is the final product of FAO pathway. We observed an increase in acetyl-CoA levels, indicating an activation of the FAO pathway. This increased acetyl-CoA formation supports ATP synthesis and promotes the production of ketone bodies [50]. The

activation of FAO relative to downstream Krebs cycle and oxidative phosphorylation further contributes to the accumulation of acetyl-CoA during the state of starvation.

Our observations also indicate a decrease in the profile of free CoA during starvation conditions. One hypothesis to support this observation is an increased utilization of CoA for fatty acid activation by formation of acyl-CoA esters and subsequent FAO processes. This reduction in free CoA levels can be associated with the higher demand for acyl-CoA formation due to the observed increase of acyl-CoA thioesters in our study. Another possible hypothesis could be the inhibition of pantothenate kinase, an enzyme responsible for catalyzing the initial biosynthetic step of free CoA. It is known that higher concentrations of long-chain acyl-CoA and acetyl-CoA can inhibit this enzyme [51]. Consequently, this inhibition of pantothenate kinase may also contribute to the decrease in CoA biosynthesis and subsequently lead to a reduction in free CoA levels.

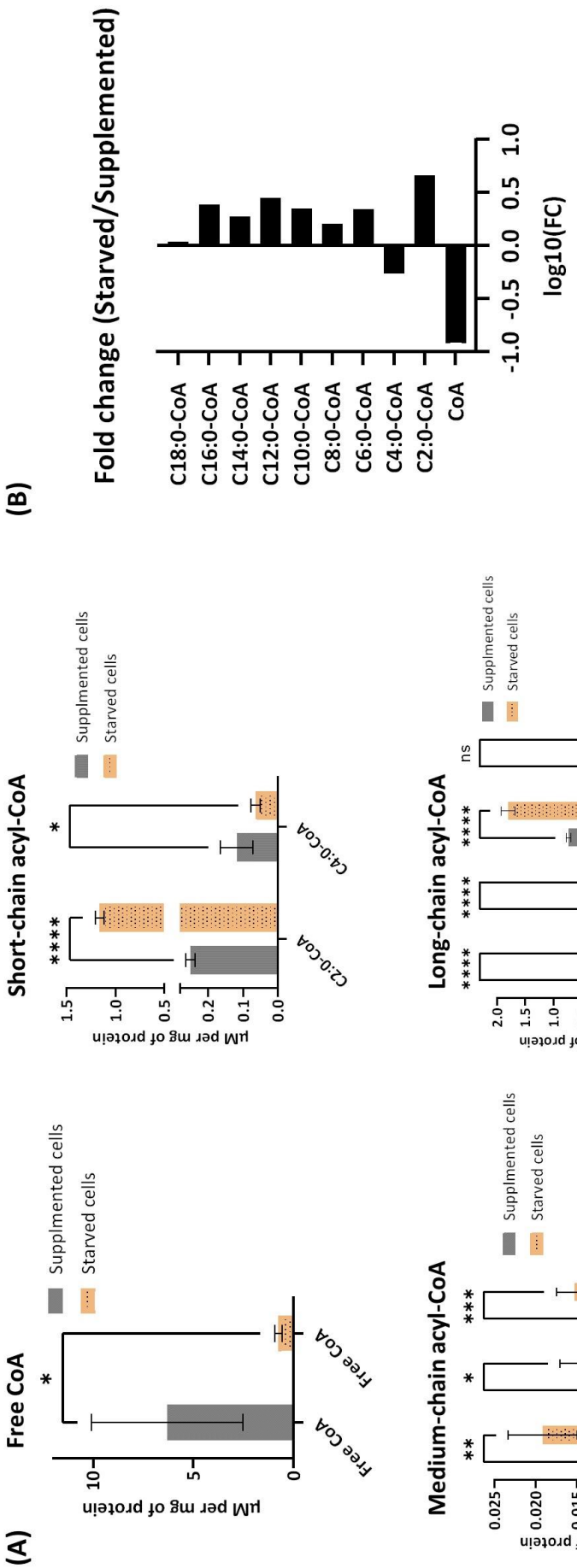

Figure 7. Acyl-CoAs profile in supplemented vs starved conditions in wildtype HepG2 cells.(A) Bar graph showing concentration (µM per mg of protein) of free CoA; short-chain acyl-CoA; medium-chain acyl-CoA and long-chain acyl-CoA in supplemented and starved state (* $p<0.05$; ** $p<0.0021$; *** $p<0.0002$; **** $p<0.0001$; ns, not significant).; (B) Fold change of acyl-CoAs in starved/supplemented conditions.

4. Conclusion

We have developed a HILIC-MS/MS method utilizing a zwitterionic ZIC-cHILIC column, covering short- to long-chain acyl-CoA species in one analytical run with the use of lower concentration of ammonium acetate. This HILIC-MS/MS method did not require the use of an ion-pairing reagent, which has several disadvantages like contamination of the MS, nor other complicated derivatization, etc. The characterization of the analytical performance was successful and the method appeared to be sensitive, linear and repeatable. We demonstrated the potential of the method by evaluating the change in acyl-CoA profile in wildtype HepG2 cells cultured in supplemented and starved state. We observed an increase in the profile of acetyl-CoA, medium- and long-chain acyl-CoA while decrease in the level of free CoA in HepG2 cells cultured in starved state. These findings suggest an increase in the fatty acid oxidation process in starved state, relative to the downstream metabolic processes.

The comprehensive analysis of acyl-CoA species in one run is highly beneficial for high-throughput analysis of biological samples and has the potential for integration in clinical settings because of its simplicity and robustness. This HILIC-MS/MS method can be further extended in the future to cover very long-chain acyl-CoA species. However, the separation and identification of isomers such as butyryl and isobutryl-CoA, succinyl-CoA and methylmalonyl-CoA, etc., or the identification of position of double bond in species such as C10:1-CoA or C18:1-CoA is the current limitation associated with this method and therefore, these species were reported by the carbon chain composition instead of their names. Hence, in future additional research should be performed for the separation of these isomeric species, which can involve exploring the use of ion-mobility mass spectrometry and electron-activated dissociation (EAD) techniques.

Author contributions

Madhulika Singh: Investigation, Conceptualization, Methodology, Data curation, Visualization, Writing – original draft & editing. Ligia Akemi Kiyuna: Methodology, Investigation, Writing – review & editing. Christoff Odendaal: Methodology, Writing – review & editing. Barbara M. Bakker: Writing – review & editing. Amy C. Harms: Supervision, Writing – review & editing. Thomas Hankemeier: Supervision, Funding acquisition, Writing – review & editing.

Declaration of competing interests

The authors declare no competing financial interests.

Acknowledgements

This work was supported by the European Union's Horizon 2020 research and innovation program under the Marie Skłodowska-Curie grant agreement PoLiMeR, No 812616; the Dutch Research Council (NWO) 'Investment Grant NWO Large' program, for the 'Building the infrastructure for Exposome research: Exposome-Scan' [No. 175.2019.032]; the NWO Netherlands X-omics Initiative [No. 184.034.019]; EXPOSOME-NL, which is funded through the Gravitation program of the Dutch Ministry of Education, Culture, and Science and the Netherlands Organization for Scientific Research (NWO grant number 024.004.017).

The authors also acknowledge Asmara Drachman, Vladimíra Cetkovská and Gaby Liem Foeng Kioen for their technical assistance.

References

[1] C.C.C.R. de Carvalho, M.J. Caramujo, The Various Roles of Fatty Acids, Molecules. 23 (2018) 2583. https://doi.org/10.3390/molecules23102583.

[2] E.P. Brass, Overview of coenzyme A metabolism and its role in cellular toxicity, Chemico-Biological Interactions. 90 (1994) 203–214. https://doi.org/10.1016/0009-2797(94)90010-8.

[3] J.L. Merritt, E. MacLeod, A. Jurecka, B. Hainline, Clinical manifestations and management of fatty acid oxidation disorders, Rev Endocr Metab Disord. 21 (2020) 479–493. https://doi.org/10.1007/s11154-020-09568-3.

[4] S.M. Houten, R.J.A. Wanders, A general introduction to the biochemistry of mitochondrial fatty acid β-oxidation, J Inherit Metab Dis. 33 (2010) 469–477. https://doi.org/10.1007/s10545-010-9061-2.

[5] P.A. Watkins, Fatty acid activation, Prog Lipid Res. 36 (1997) 55–83. https://doi.org/10.1016/s0163-7827(97)00004-0.

[6] J.M. Ellis, C.E. Bowman, M.J. Wolfgang, Metabolic and Tissue-Specific Regulation of Acyl-CoA Metabolism, PLOS ONE. 10 (2015) e0116587. https://doi.org/10.1371/journal.pone.0116587.

[7] Q. Li, S. Zhang, J.M. Berthiaume, B. Simons, G.-F. Zhang, Novel approach in LC-MS/MS using MRM to generate a full profile of acyl-CoAs: discovery of acyl-dephospho-CoAs, J Lipid Res. 55 (2014) 592–602. https://doi.org/10.1194/jlr.D045112.

[8] T.J. Grevengoed, E.L. Klett, R.A. Coleman, Acyl-CoA Metabolism and Partitioning, Annu Rev Nutr. 34 (2014) 1–30. https://doi.org/10.1146/annurev-nutr-071813-105541.

[9] T. Migita, K. Takayama, T. Urano, D. Obinata, K. Ikeda, T. Soga, S. Takahashi, S. Inoue, ACSL3 promotes intratumoral steroidogenesis in prostate cancer cells, Cancer Sci. 108 (2017) 2011–2021. https://doi.org/10.1111/cas.13339.

[10] S. Zhang, O.D. Nelson, I.R. Price, C. Zhu, X. Lu, I.R. Fernandez, R.S. Weiss, H. Lin, Long-chain fatty acyl coenzyme A inhibits NME1/2 and regulates cancer metastasis, Proceedings of the National Academy of Sciences. 119 (2022) e2117013119. https://doi.org/10.1073/pnas.2117013119.

[11] S. Jackowski, R. Leonardi, Deregulated Coenzyme A, Loss of Metabolic Flexibility and Diabetes, Biochem Soc Trans. 42 (2014) 1118–1122. https://doi.org/10.1042/BST20140156.

[12] J.E. Kanter, F. Kramer, S. Barnhart, M.M. Averill, A. Vivekanandan-Giri, T. Vickery, L.O. Li, L. Becker, W. Yuan, A. Chait, K.R. Braun, S. Potter-Perigo, S. Sanda, T.N. Wight, S. Pennathur, C.N. Serhan, J.W. Heinecke, R.A. Coleman, K.E. Bornfeldt, Diabetes promotes an inflammatory macrophage phenotype and atherosclerosis through acyl-CoA synthetase 1, Proceedings of the National Academy of Sciences. 109 (2012) E715–E724. https://doi.org/10.1073/pnas.1111600109.

[13] A. Michno, A. Raszeja-Specht, A. Jankowska-Kulawy, T. Pawelczyk, A. Szutowicz, Effect of L-Carnitine on Acetyl-CoA Content and Activity of Blood Platelets in Healthy and Diabetic Persons, Clinical Chemistry. 51 (2005) 1673–82. https://doi.org/10.1373/clinchem.2005.050328.

[14] S. HORIE, M. ISOBE, T. SUGA, Changes in CoA Pools in Hepatic Peroxisomes of the Rat, under Various Conditions, The Journal of Biochemistry. 99 (1986) 1345–1352. https://doi.org/10.1093/oxfordjournals.jbchem.a135602.

[15] P. Li, M. Gawaz, M. Chatterjee, M. Lämmerhofer, Targeted Profiling of Short-, Medium-, and Long-Chain Fatty Acyl-Coenzyme As in Biological Samples by Phosphate Methylation Coupled to Liquid Chromatography–Tandem Mass Spectrometry, Anal. Chem. 93 (2021) 4342–4350. https://doi.org/10.1021/acs.analchem.1c00664.
[16] L. Gao, W. Chiou, H. Tang, X. Cheng, H. Camp, D. Burns, Simultaneous quantification of malonyl-CoA and several other short-chain acyl-CoAs in animal tissues by ion-pairing reversed-phase HPLC/MS, Journal of Chromatography. B, Analytical Technologies in the Biomedical and Life Sciences. 853 (2007) 303–13. https://doi.org/10.1016/j.jchromb.2007.03.029.
[17] S. Wang, Z. Wang, L. Zhou, X. Shi, G. Xu, Comprehensive Analysis of Short-, Medium-, and Long-Chain Acyl-Coenzyme A by Online Two-Dimensional Liquid Chromatography/Mass Spectrometry, Anal Chem. 89 (2017) 12902–12908. https://doi.org/10.1021/acs.analchem.7b03659.
[18] X. Yang, Y. Ma, N. Li, H. Cai, M.G. Bartlett, Development of a Method for the Determination of Acyl-CoA Compounds by Liquid Chromatography Mass Spectrometry to Probe the Metabolism of Fatty Acids, Anal. Chem. 89 (2017) 813–821. https://doi.org/10.1021/acs.analchem.6b03623.
[19] L.G. Rivera, M.G. Bartlett, Chromatographic methods for the determination of acyl-CoAs, Anal. Methods. 10 (2018) 5252–5264. https://doi.org/10.1039/C8AY01472H.
[20] P.G. Tardi, J.J. Mukherjee, P.C. Choy, The quantitation of long-chain acyl-CoA in mammalian tissue, Lipids. 27 (1992) 65–67. https://doi.org/10.1007/BF02537062.
[21] G. Liu, J. Chen, P. Che, Y. Ma, Separation and Quantitation of Short-Chain Coenzyme A's in Biological Samples by Capillary Electrophoresis, Anal. Chem. 75 (2003) 78–82. https://doi.org/10.1021/ac0261505.
[22] A. Demoz, A. Garras, D.K. Asiedu, B. Netteland, R.K. Berge, Rapid method for the separation and detection of tissue short-chain coenzyme A esters by reversed-phase high-performance liquid chromatography, Journal of Chromatography B: Biomedical Sciences and Applications. 667 (1995) 148–152. https://doi.org/10.1016/0378-4347(94)00595-V.
[23] X. Liu, S. Sadhukhan, S. Sun, G.R. Wagner, M.D. Hirschey, L. Qi, H. Lin, J.W. Locasale, High-Resolution Metabolomics with Acyl-CoA Profiling Reveals Widespread Remodeling in Response to Diet, Mol Cell Proteomics. 14 (2015) 1489–1500. https://doi.org/10.1074/mcp.M114.044859.
[24] M. Singh, H.L. Elfrink, A.C. Harms, T. Hankemeier, Recent developments in the analytical approaches of acyl-CoAs to assess their role in mitochondrial fatty acid oxidation disorders, Molecular Genetics and Metabolism. (2023) 107711. https://doi.org/10.1016/j.ymgme.2023.107711.
[25] A.E. Jones, N.J. Arias, A. Acevedo, S.T. Reddy, A.S. Divakaruni, D. Meriwether, A Single LC-MS/MS Analysis to Quantify CoA Biosynthetic Intermediates and Short-Chain Acyl CoAs, Metabolites. 11 (2021) 468. https://doi.org/10.3390/metabo11080468.
[26] L. Abrankó, G. Williamson, S. Gardner, A. Kerimi, Comprehensive quantitative analysis of fatty-acyl-Coenzyme A species in biological samples by ultra-high performance liquid chromatography–tandem mass spectrometry harmonizing hydrophilic interaction and reversed phase chromatography, Journal of Chromatography A. 1534 (2018) 111–122. https://doi.org/10.1016/j.chroma.2017.12.052.
[27] N.W. Snyder, S.S. Basu, Z. Zhou, A.J. Worth, I.A. Blair, Stable isotope dilution liquid chromatography-mass spectrometry analysis of cellular and tissue medium- and long-chain acyl-coenzyme A thioesters, Rapid Commun Mass Spectrom. 28 (2014) 1840–1848. https://doi.org/10.1002/rcm.6958.
[28] S. Neubauer, D.B. Chu, H. Marx, M. Sauer, S. Hann, G. Koellensperger, LC-MS/MS-based analysis of coenzyme A and short-chain acyl-coenzyme A thioesters, Anal Bioanal Chem. 407 (2015) 6681–6688. https://doi.org/10.1007/s00216-015-8825-9.
[29] S.M. Lam, T. Zhou, J. Li, S. Zhang, G.H. Chua, B. Li, G. Shui, A robust, integrated platform for comprehensive analyses of acyl-coenzyme As and acyl-carnitines revealed chain length-dependent disparity in fatty acyl metabolic fates across Drosophila development, Science Bulletin. 65 (2020) 1840–1848. https://doi.org/10.1016/j.scib.2020.07.023.
[30] M. Holcapek, K. Volná, P. Jandera, L. Kolárová, K. Lemr, M. Exner, A. Církva, Effects of ion-pairing reagents on the electrospray signal suppression of sulphonated dyes and intermediates, J Mass Spectrom. 39 (2004) 43–50. https://doi.org/10.1002/jms.551.
[31] B. Buszewski, S. Noga, Hydrophilic interaction liquid chromatography (HILIC)--a powerful separation technique, Anal Bioanal Chem. 402 (2012) 231–247. https://doi.org/10.1007/s00216-011-5308-5.
[32] R. Li, J. Huang, Chromatographic behavior of epirubicin and its analogues on high-purity silica in hydrophilic interaction chromatography, J Chromatogr A. 1041 (2004) 163–169. https://doi.org/10.1016/j.chroma.2004.04.033.
[33] P. Hemström, K. Irgum, Hydrophilic interaction chromatography, Journal of Separation Science. 29 (2006) 1784–1821. https://doi.org/10.1002/jssc.200600199.
[34] H. Wu, A.D. Southam, A. Hines, M.R. Viant, High-throughput tissue extraction protocol for NMR- and MS-based metabolomics, Anal Biochem. 372 (2008) 204–212. https://doi.org/10.1016/j.ab.2007.10.002.

[35] T. Van Der Laan, A.-C. Dubbelman, K. Duisters, A. Kindt, A.C. Harms, T. Hankemeier, High-Throughput Fractionation Coupled to Mass Spectrometry for Improved Quantitation in Metabolomics, Anal. Chem. 92 (2020) 14330–14338. https://doi.org/10.1021/acs.analchem.0c01375.

[36] N. Kadian, K.S.R. Raju, M. Rashid, M.Y. Malik, I. Taneja, M. Wahajuddin, Comparative assessment of bioanalytical method validation guidelines for pharmaceutical industry, Journal of Pharmaceutical and Biomedical Analysis. 126 (2016) 83–97. https://doi.org/10.1016/j.jpba.2016.03.052.

[37] D. Wolrab, M. Chocholoušková, R. Jirásko, O. Peterka, M. Holčapek, Validation of lipidomic analysis of human plasma and serum by supercritical fluid chromatography-mass spectrometry and hydrophilic interaction liquid chromatography-mass spectrometry, Anal Bioanal Chem. 412 (2020) 2375–2388. https://doi.org/10.1007/s00216-020-02473-3.

[38] M. Azim, M. Moloy, P. Bhasin, HPLC METHOD DEVELOPMENT AND VALIDATION: A REVIEW, International Research Journal of Pharmacy. 4 (2015) 39–46. https://doi.org/10.7897/2230-8407.04407.

[39] merck_sequant-zic-chilic_brochure.pdf, (n.d.). https://mz-at.de/fileadmin/user_upload/Brochures/merck_sequant-zic-chilic_brochure.pdf (accessed June 8, 2023).

[40] F. Hosseinkhani, L. Huang, A.-C. Dubbelman, F. Guled, A.C. Harms, T. Hankemeier, Systematic Evaluation of HILIC Stationary Phases for Global Metabolomics of Human Plasma, Metabolites. 12 (2022) 165. https://doi.org/10.3390/metabo12020165.

[41] S. Arase, S. Kimura, T. Ikegami, Method optimization of hydrophilic interaction chromatography separation of nucleotides using design of experiment approaches I: Comparison of several zwitterionic columns, J Pharm Biomed Anal. 158 (2018) 307–316. https://doi.org/10.1016/j.jpba.2018.05.014.

[42] E. Zborníková, Z. Knejzlík, V. Hauryliuk, L. Krásný, D. Rejman, Analysis of nucleotide pools in bacteria using HPLC-MS in HILIC mode, Talanta. 205 (2019) 120161. https://doi.org/10.1016/j.talanta.2019.120161.

[43] A. Wakamatsu, K. Morimoto, M. Shimizu, S. Kudoh, A severe peak tailing of phosphate compounds caused by interaction with stainless steel used for liquid chromatography and electrospray mass spectrometry, Journal of Separation Science. 28 (2005) 1823–1830. https://doi.org/10.1002/jssc.200400027.

[44] J. Zhang, Q. Wang, B. Kleintop, T. Raglione, Suppression of peak tailing of phosphate prodrugs in reversed-phase liquid chromatography, Journal of Pharmaceutical and Biomedical Analysis. 98 (2014) 247–252. https://doi.org/10.1016/j.jpba.2014.05.027.

[45] H.-L. Koh, A.-J. Lau, E.C.-Y. Chan, Hydrophilic interaction liquid chromatography with tandem mass spectrometry for the determination of underivatized dencichine (beta-N-oxalyl-L-alpha,beta-diaminopropionic acid) in Panax medicinal plant species, Rapid Commun Mass Spectrom. 19 (2005) 1237–1244. https://doi.org/10.1002/rcm.1928.

[46] I. Kohler, M. Verhoeven, R. Haselberg, A.F.G. Gargano, Hydrophilic interaction chromatography – mass spectrometry for metabolomics and proteomics: state-of-the-art and current trends, Microchemical Journal. 175 (2022) 106986. https://doi.org/10.1016/j.microc.2021.106986.

[47] Y. Du, Y. Li, X. Hu, X. Deng, Z. Qian, Z. Li, M. Guo, D. Tang, Development and evaluation of a hydrophilic interaction liquid chromatography-MS/MS method to quantify 19 nucleobases and nucleosides in rat plasma, Biomedical Chromatography. 31 (2017) e3860. https://doi.org/10.1002/bmc.3860.

[48] X. Liu, Z. Ser, J.W. Locasale, Development and Quantitative Evaluation of a High-Resolution Metabolomics Technology, Anal. Chem. 86 (2014) 2175–2184. https://doi.org/10.1021/ac403845u.

[49] M.-H. Ryu, J.W. Daily, Y.-S. Cha, Effect of starvation on hepatic acyl-CoA synthetase, carnitine palmitoyltransferase-I, and acetyl-CoA carboxylase mRNA levels in rats, Nutrition. 21 (2005) 537–542. https://doi.org/10.1016/j.nut.2004.08.015.

[50] L. Shi, B.P. Tu, Acetyl-CoA and the Regulation of Metabolism: Mechanisms and Consequences, Curr Opin Cell Biol. 33 (2015) 125–131. https://doi.org/10.1016/j.ceb.2015.02.003.

[51] Y.-M. Zhang, C.O. Rock, S. Jackowski, Feedback Regulation of Murine Pantothenate Kinase 3 by Coenzyme A and Coenzyme A Thioesters, Journal of Biological Chemistry. 280 (2005) 32594–32601. https://doi.org/10.1074/jbc.M506275200.

Supplementary material

Table S1. Gradient table for HILIC-TOF-MS chromatographic separation of acyl-CoAs in high-resolution mode.

Time (min)	Flow rate (mL min^{-1})	MP-A (%)	MP-B (%)
Initial	0.25	100	0
2.3	0.25	100	0
14	0.25	25	75
15.5	0.25	25	75
15.6	0.25	0	100
17.5	0.25	0	100
18.5	0.25	100	0
20	0.25	100	0

Table S2. Concentration (µM) of non-endogenous standards used for preparing the calibration curves for validation.

Standards	cal-1	cal-2	cal-3	cal-4	cal-5	cal-6	cal-7	cal-8
C2:0-CoA($^{13}C_2$)	0.042	0.063	0.117	0.193	0.386	0.964	3.396	10.410
C7:0-CoA	0.039	0.059	0.108	0.178	0.356	0.890	3.133	9.604
C15:0-CoA	0.013	0.019	0.035	0.058	0.117	0.292	1.028	3.150
C17:0-CoA	0.034	0.051	0.093	0.154	0.308	0.769	2.708	8.302

Table S3. Accurate and observed m/z values of representative acyl-CoA standards in protonated **$[M+H]^+$**, deprotonated **$[M-H]^-$** and doubly charged **$[M-2H]^{2-}$** ionization modes.

Standards	$[M+H]^+$		$[M-H]^-$		$[M-H]^{2-}$	
	Accurate mass	Observed mass	Accurate mass	Observed mass	Accurate mass	Observed masss
C2:0-CoA	**810.133**	810.140	**808.119**	808.123	**403.556**	403.551
C8:0-CoA	**894.227**	894.234	**892.212**	892.211	**445.603**	445.607
C16:0-CoA	**1006.352**	1006.362	**1004.338**	1004.338	**501.665**	501.666
C18:1-CoA	**1032.368**	1032.367	**1030.353**	1030.353	**514.673**	514.678

Table S4. Accurate and observed m/z values with the retention time of the targets in protonated **$[M+H]^+$** form.

Free CoA/Acyl-CoA Species	Accurate $[M+H]^+$	Observed $[M+H]^+$	Retention Time (min)
Free CoA	768.12378	768.1254	6.52
C2:0-CoA	810.1331	810.136	6.44
C3:0-CoA	824.1487	824.1458	6.39
C4:0-CoA	838.1644	838.1579	6.35
C6:0-CoA	866.1957	866.193	6.3
C8:0-CoA	894.227	894.2336	6.09
C10:0-CoA	922.2583	922.2548	6
C12:0-CoA	950.2896	950.2924	5.91
C14:0-CoA	978.3209	978.3266	5.84
C16:0-CoA	1006.3522	1006.35	5.78
C18:0-CoA	1034.3835	1034.3823	5.75

Table S5. Deviation in the peak area of non-endogenous acyl-CoA standards over 3 days after storing at -80 °C.

Non-endogenous acyl-CoA standards	Area measured on day-1	Area measured on day-3	RSD (%)
C2:0-CoA($^{13}C_2$)	2.14E+06	2.38E+06	7.61
C7:0-CoA	3.53E+06	4.07E+06	10.07
C15:0-CoA	1.02E+06	9.35E+05	5.86
C17:0-CoA	8.10E+05	7.34E+05	6.94

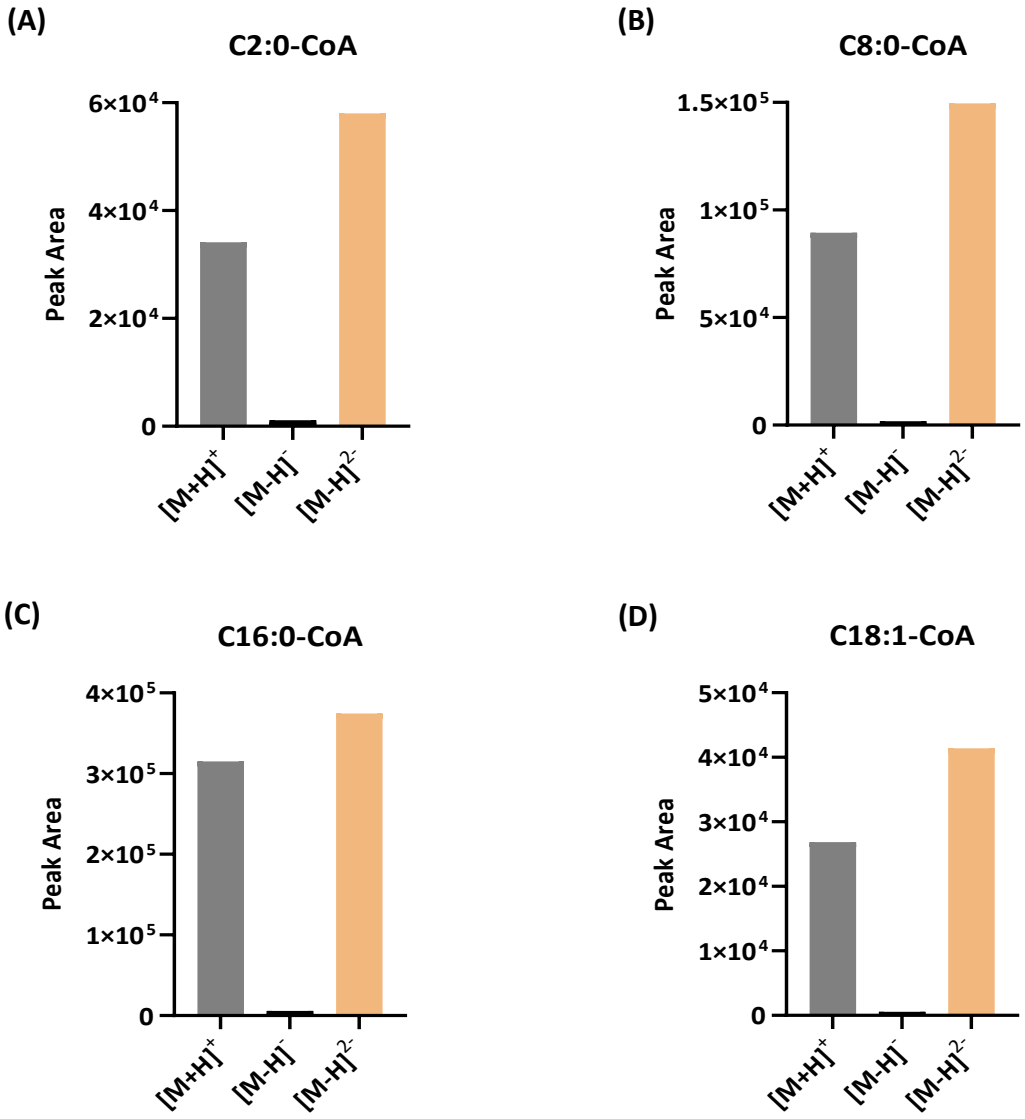

Figure S1. Sensitivity of representative acyl-CoA standards in positive and negative ion mode. (A) C2:0-CoA; (B) C8:0-CoA; (C) C16:0-CoA; (D) C18:1-CoA.

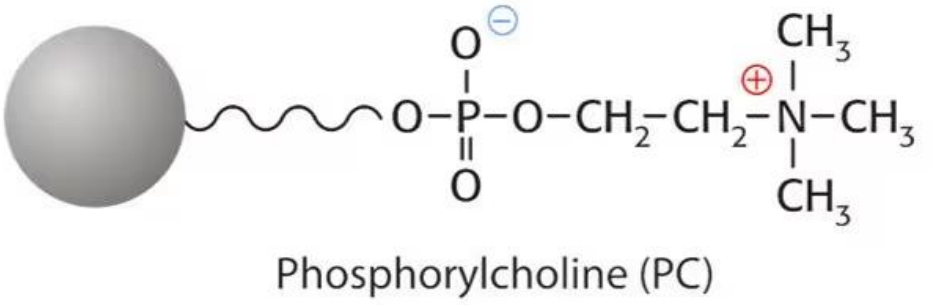

Figure S2. Zwitterionic stationary phase of ZIC-cHILIC column consists of phosphorylcholine group.

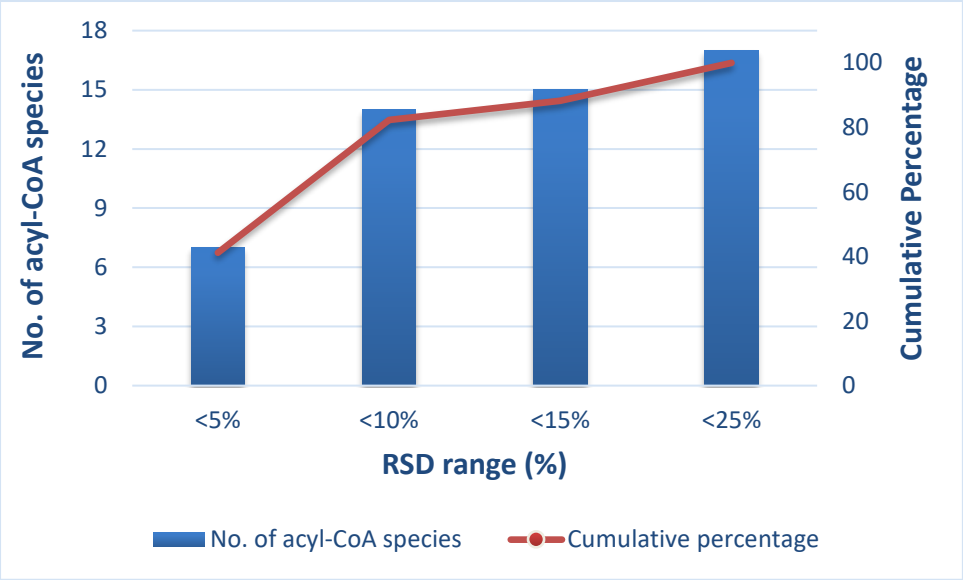

Figure S3. Repeatability of identified acyl-CoA species in HepG2 cells.